Fuel 358 (2024) 130169

Contents lists available at ScienceDirect

Fuel

journal homepage: www.elsevier.com/locate/fuel

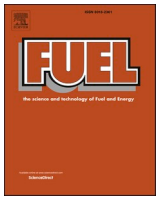

Full Length Article

Droplet characterization of a pressure-swirl atomizer by means of high-fidelity modelling based on DNS simulations

F.J. Salvador [a,*], P. Martí-Aldaraví [a], A. Lozano [a], H. Taghavifar [b], A. Nemati [c]

[a] CMT-Motores Térmicos, Universitat Politècnica de València, Camino de Vera s/n, E-46022 Valencia, Spain
[b] Department of Technology and Safety, UiT the Arctic University of Norway, Tromsø, Norway
[c] Department of Energy Conversion and Storage, Technical University of Denmark, Fysikvej, DK-2800 Kgs. Lyngby, Denmark

ARTICLE INFO

Keywords:
Atomization
DNS
Two-phase flow
Spray
Pressure-swirl
Droplet

ABSTRACT

Liquid injection optimization is key to enhance the efficiency of many processes in a wide variety of fields. Combustion processes are one of the most challenging ones, due to the direct emissions and greenhouse gases implications. This work aims at studying the external two-phase flow produced when injecting fuel with a pressure-swirl atomizer in an operating condition typical of an academic burner. The main objective is to have a better comprehension of the atomization process in this type of nozzles, getting information on the droplets' characteristic size and how they are produced and arranged. For that regard, a high-fidelity Direct Numerical Simulation (DNS) is used to analyse the very near field of the spray produced, where primary atomization takes place. Pre-processing tasks are explained in terms of geometry comprehension, computational domain and mesh selection, boundary conditions and main simulation setup parameters. Then, through post-processing tasks, both quantitative and qualitative results are extracted, which will serve to validate the modelling against previous works and to provide novel data about the atomization process in pressure-swirl atomizers. Results show that smaller droplets predominate over bigger ones as expected, since just the first millimetres of the spray are modelled. However, there is a clear trend of droplet's size growing when increasing both axial and radial distances, indicating coalescence in regions relatively far from the nozzle. The achieved results, together with results from simulating the injection event with other fuels or at other operating conditions, can be used to develop a phenomenological model able to predict how atomization is going to be as a function of the non-dimensional Reynolds and Weber numbers that could be implemented in lower-resolution RANS and LES codes for modelling atomization. This investigation proves that it is possible to faithfully predict the near field of these sprays through DNS simulation, getting similar trends to those of the experimental data, and that the study through numerical models is necessary in the investigation process. The information they can bring, together with the experimental knowledge, can make a good synergy that will eventually lead to a better understanding of this type of atomizers.

1. Introduction

One of the biggest concerns regarding combustion processes is the impact of pollutants on public health and climate change. Nowadays, important industries, such as the aeronautical field, in which this work is developed, still need combustion engines to achieve their mission in a safe way due to the high specific power demanded. Another example is energy generation, transitioning progressively to eco-friendly production methods but still with a remarkable percentage of combustion-based generation. Because of that, the optimization of the combustion process turns out to be fundamental when looking for pollutant and fuel consumption reduction.

In this context, fuel injection plays a key role due to its direct influence on pollutant formation. Liquid fuel is injected into the engine combustion chamber through an atomizer, which must quickly break it up into ligaments and droplets to promote fast evaporation and a homogeneous air–fuel mixture, increasing combustion efficiency and reducing pollutant emissions. Within this process, primary atomization has a significant impact on droplet generation and distribution and, therefore, on air–fuel mixing and on the combustion process itself. To clarify this phenomenon, spray formation needs to be investigated from both computational and experimental standpoints.

Focusing on aeronautical applications, there have been a lot of innovative solutions over time for the atomizer design that improve the primary atomization process with respect to classical round-jet

* Corresponding author.
E-mail address: fsalvado@mot.upv.es (F.J. Salvador).

https://doi.org/10.1016/j.fuel.2023.130169
Received 8 May 2023; Received in revised form 6 October 2023; Accepted 22 October 2023
Available online 31 October 2023

Nomenclature

Re	Reynolds number
RANS	Reynolds-Averaged Navier-Stokes
LES	Large Eddy Simulation
PDA	Phase Doppler Anemometry
LDA	Laser Doppler Anemometry
PIV	Particle Image Velocimetry
VOF	Volume Of Fluid
DNS	Direct Numerical Simulation
CT-Scan	Computed Tomography Scan
SEM	Scanning Electron Microscope
AMR	Adaptive Mesh Refinement
CFL	Courant-Friedrichs-Lewy number
RMS	Root Mean Square
PDF	Probability Density Function
D_0	Nozzle's discharge orifice diameter
$\boldsymbol{u}$	Velocity vector
u	Axial velocity
v	Radial velocity
w	Azimuthal velocity
p	Pressure
$\boldsymbol{D}$	Deformation tensor
$\boldsymbol{n}$	Normal to the liquid–gas interface vector
f	Liquid volume fraction field
$l_{x,y,z}$	Cubic domain's side size
$n_{ref,max}$	Maximum refinement level
$d_{x,min}$	Minimum cell size
$n_{cells,0}$	Number of cells at $t = 0$
dt	Time step
t_{simu}	Total simulated time
L	Characteristic length
SN	Swirl Number
G_{tq}	Flow rate of the tangential momentum's axial component over the axial cross-section
G_{ax}	Flow rate of the axial momentum's axial component across the axial cross-section
R	Nozzle's outer radius
r	Radial position
x	Axial position
t	Time
d	Droplet diameter

Greek symbols

ρ	Density
μ	Dynamic viscosity
σ	Surface tension
κ	Interface curvature
δ_s	Dirac distribution function
η	Kolmogorov scale
α	Threshold for iso-surface representation in Paraview
θ	Spray's spread angle

atomizers [1]. Airblast atomizers [2] are the most extended solutions in the aero-engines current state of the art, but often working together with a simplex pressure-swirl atomizer in several configurations. The latter kind, which is the one to be studied here, is generally used to generate the pilot flame for startup purposes and low-power regimes [3].

Simplex pressure-swirl atomizers are interesting solutions, as they provide a swirling hollow cone of liquid that promotes earlier atomization once injected into the combustion chamber. These atomizers' way of working is illustrated in Fig. 1. Fuel is supplied into a spin chamber through tangential ports. This way, the fuel gets a swirling motion that is able to generate a depression in the centre of the chamber if the Reynolds number is high enough, drawing air in from the outside of the atomizer. When this happens, the so-called "air core" generated inside the injector forces the liquid fuel to adhere to the walls producing a film, which is injected into the combustion chamber in the shape of a hollow cone thanks to the non-negligible radial and azimuthal velocities. The swirling motion of the injected fuel film, together with its interaction with the surrounding air (part of it being drawn inside the nozzle), helps to promote atomization in the near field of the spray and to enhance the air–fuel mixing compared to classical round-jet atomizers.

One important consequence derived from the advantages of these

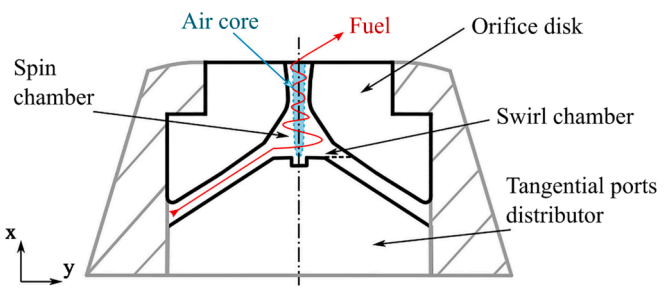

Fig. 1. Cross-section of the outlet part of a simplex pressure-swirl atomizer and paths for the fuel (red line) and air (blue) [4].

type of atomizers in terms of atomization and air–fuel mixing is that, thanks to the swirling-hollow-cone spray injected, the near-nozzle field presents a less-dense liquid zone. Another positive point is that this kind of injector, besides for combustion applications, is widely used in agricultural, pharmaceutical, painting, spray cooling and firefighting applications, among others [4]. Thus, many fields would be benefited by the investigation and better understanding of simplex pressure-swirl atomizers.

To be able to study the external flow of a simplex pressure-swirl atomizer in detail, it is important to properly characterize the internal flow which, in this type of nozzles, governs the behaviour of the liquid sheet at the discharge orifice. In this regard, the air core developed inside the nozzle plays a key role, directly affecting the subsequent primary breakup. Some theoretical models have been proposed to justify important variables such as the discharge coefficient, air core radius (which eventually defines the liquid sheet thickness at the nozzle and its variability) and spread angle [5]. In [6], the effect of fuel temperature on the air core stability was studied, defining unstable, transitional and stable regimes based on the non-dimensional Reynolds number (Re). From the numerical standpoint, Reynolds-Averaged Navier-Stokes (RANS) simulations were computed in [7] to determine the topology of the air core and the velocity components inside the nozzle. Recently, in [4], Large Eddy Simulation (LES) computations of the internal flow were carried out to solve the velocity and volume fraction fields at the discharge orifice and use them as initial boundary conditions for spray modelling, thus providing a more realistic inflow for the external flow simulation.

Regarding the external flow, both experimental and modelling works have been done to better understand atomization process in simplex pressure-swirl atomizers. As far as the experimental part is concerned, a wide variety of visualization techniques have been employed, such as Mie-scattering [8], Phase Doppler Anemometry (PDA) [9], Laser Doppler Anemometry (LDA) [10] or Particle Image Velocimetry (PIV) [11]. In [12], microscopic shadowgraphy was used to visualize the spray produced by a simplex pressure-swirl atomizer and post-processing techniques were developed to extract the spread angle, contours of the

liquid phase and droplet size. However, quantitative analyses by experimental means are difficult to accomplish in the very near-nozzle region because of the dense spray which, although possible, is still difficult to visualize in detail with the current optical techniques. Thus, results are not as reliable as those obtained in the secondary breakup region. It is in that near region where numerical simulations can help to comprehend the atomization phenomena, bridging the gap between the near and the far field.

From the numerical standpoint, RANS and LES have been the most used tools to characterize the external flow in this type of atomizer, using in most cases Volume of Fluid (VOF) methods to deal with the interface between fluids. In [13], a commercial RANS code was used to predict the main characteristics of the internal flow, detecting fuel cavitation in the pressure drop zone of the air core (bottom part) for injection pressures sufficiently high. In [14], LES simulations of the two-phase flow were done carrying out a Reynolds number sweep to investigate the link between the inner nozzle flow and the liquid sheet characteristics in laminar, transitional and fully turbulent conditions. They were able to find that a certain Reynolds number of the fuel inside the nozzle is needed to generate to the hollow-cone spray type. In the last two studies mentioned, both the internal and external flow were simulated simultaneously, meaning that the level of detail in the resolution of the spray was lower than in studies fully focused on external flow. For that reason, the authors did not fully capture the main triggers that lead to primary breakup. Works by means of Direct Numerical Simulation (DNS) should be capable of capturing them but are scarcer. In [15], a DNS multiphase flow model through VOF methodology is used to analyse the evolution and fragmentation of the spray, concluding that the primary breakup is caused by the injected liquid film instabilities when interacting with the surrounding air and that the first outcome of that breakup are ligaments instead of spherical droplets. Furthermore, in [16], the authors also use DNS to model the external flow but using a Level Set method instead of VOF for interface capturing. They compare the results given by using both laminar and turbulent inflow conditions, getting a better breakup efficiency with the turbulent ones and pointing out the importance of prescribing realistic turbulent inflow boundary conditions in order to faithfully reproduce the atomization phenomena, highlighting the important role of turbulence on the process.

The objective of this work is to numerically study the droplet population generated by the primary atomization taking place in a simplex pressure-swirl atomizer at a high level of detail by means of Direct Numerical Simulation. In this case, the Danfoss atomizer geometry analysed in [4] will be investigated for the same operating condition than in the configuration studied in the Turbulent Combustion of Sprays workshops [17], for which there is a certain amount of experimental work behind [12,18]. This investigation thus aims at shedding light on that near region where quantitative experimental results are more difficult to obtain. To achieve that, first, a description of the aforementioned geometry is done in Section 2 as part of the pre-processing work. Then, a brief explanation of the numerical methods used by the code employed to solve this problem can be found in Section 3, as well as the operating condition that is simulated. In Section 4, the main features of the simulation are presented, including the spatial domain, the computational mesh and the boundary conditions, with special focus on the inflow ones. Section 5 discusses the results, analysing spray morphology and development, validating results with previous works and, lastly, describing some features obtained regarding droplets population. Finally, Section 6 summarizes the main conclusions extracted from this work.

2. Geometry description

Before carrying out any numerical problem, pre-processing tasks must be done to prepare and configure the case properly. The first one is to know the relevant geometry for the intended study. Although it is an external flow problem and only the nozzle diameter is necessary to configure the numerical case in terms of geometry, it is important to know as much information of the atomizer as possible, both from a geometrical and from a working principle point of view. That information will help to better understand the behaviour of the injection and atomization processes.

The atomizer geometry to be studied here is the one mounted in the CORIA Rouen Spray Burner, which is used for academic purposes. It is a commercial Danfoss OD-H 030H8103 oil nozzle, which is a hollow-cone atomizer manufactured according to European standard EN 293. Its nominal characteristics are a spread angle of 80° and a mass flow rate of 1.35 kg/h [19]. A picture of this injector is shown in Fig. 2.

In Fig. 1 and Fig. 2, it can be seen that the tangential ports distributor and the orifice disk, two of the solid pieces that make up the injector, shape the internal geometry of the Danfoss atomizer. The result is a series of internal channels and chambers that make it possible to prepare the flow for the hollow-cone type spray. Those are three tangential inlet fuel ports, from where fuel is fed, the swirl and spin chambers, where fuel acquires the rotatory motion, and the discharge orifice from where fuel is injected into the combustion chamber.

In [4], a thorough determination of this atomizer's geometry was done using a combination of experimental techniques to visualize and measure all the aforementioned pieces. Specifically, Computed Tomography Scan (CT-Scan), optical microscope visualization and Scanning Electron Microscope (SEM) visualization were used. The different geometrical parameters measured are depicted in Fig. 3 and Table 1. The reader is referred to that work to find the detailed geometrical information.

As stated at the beginning of this section, just the diameter of the discharge orifice is going to be indicated by its importance in this study, being $D_0 = 300$ μm.

Another important part of the pre-processing work is to know the operating condition in which the injection will be simulated, regarding the fluids that will take part in the process (fuel and air) and their properties, their characteristic velocities at the nozzle exit, as well as the gas conditions at the discharge chamber. All these details will be discussed in the next section.

3. Numerical methods

In this section, a brief description of the code used to carry out the numerical study of the external flow produced by the Danfoss pressure-swirl atomizer is presented in Subsection 3.1. Specifically, the main equations solved by the DNS code and the principles of the adaptive mesh techniques used for spatially discretize the computational domain are explained. In Subsection 3.2, the operating condition to be simulated is detailed regarding fuel and air properties and average injection velocities.

3.1. Code outline

The computations were performed using the open-source code Basilisk [20]. It is a C language-based code for DNS simulations of 1D/2D/3D compressible/incompressible flows that solves partial differential equations on adaptive cartesian meshes. Hence, it uses Adaptive Mesh Refinement (AMR) techniques which makes it possible to compute multi-scale problems with high level of detail.

For cases like the one to be solved here, the code simulates a multiphase incompressible flow using the mass and momentum conservation equations, namely Navier-Stokes equations for viscous fluid problems, indicated below:

$$\nabla \cdot \boldsymbol{u} = 0 \tag{1}$$

$$\rho[\partial_t \boldsymbol{u} + \nabla \cdot (\boldsymbol{u} \otimes \boldsymbol{u})] = -\nabla p + \nabla \cdot (2\mu \boldsymbol{D}) + \sigma \kappa \delta_s \boldsymbol{n} \tag{2}$$

where the second term on the left-hand side of Eq. (2) is the velocity

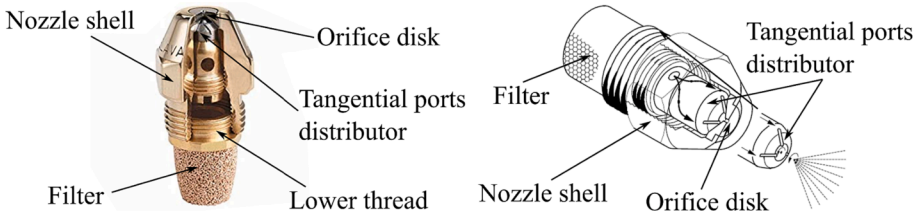

Fig. 2. Picture and sketch of the Danfoss OD-H nozzle [19].

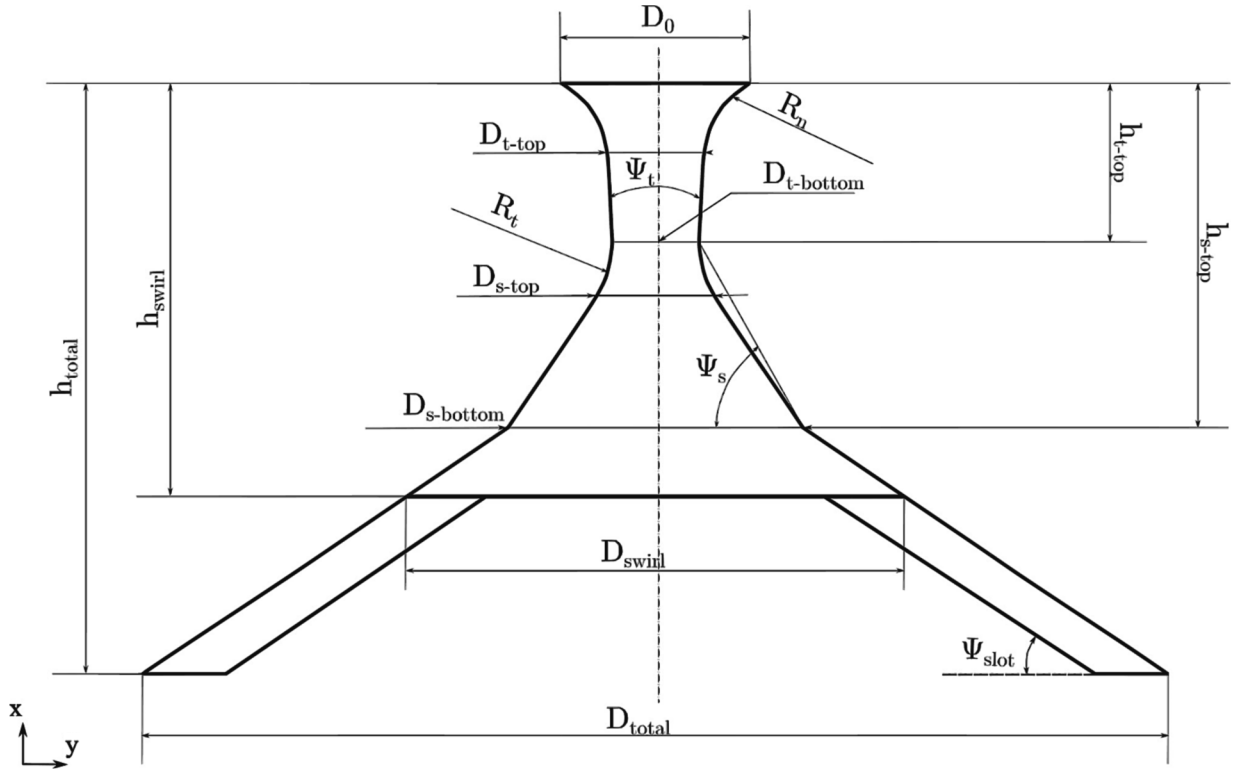

Fig. 3. Danfoss internal geometry parameters characterized in [4].

Table 1
Values of the Danfoss atomizer internal geometry parameters [4].

Parameter	Unit	Value
D_0	μm	300
$D_{t\text{-}top}$	μm	180
$D_{t\text{-}bottom}$	μm	165
$D_{s\text{-}top}$	μm	210
$D_{s\text{-}bottom}$	μm	500
D_{swirl}	μm	780
D_{total}	μm	3375
$h_{t\text{-}top}$	μm	240
$h_{s\text{-}top}$	μm	540
h_{swirl}	μm	620
h_{total}	μm	2400
R_n	μm	308
R_t	μm	190
Ψ_t	°	6
Ψ_s	°	61
Ψ_{slot}	°	30

advection term and $\boldsymbol{D}$ is the deformation tensor:

$$\boldsymbol{D} = [\nabla \boldsymbol{u} + (\nabla \boldsymbol{u})^T]/2 \tag{3}$$

In these expressions, $\boldsymbol{u} = (u,v,w)$ is the velocity field, p is the pressure field, $\rho \equiv \rho(x,t)$ is the fluid density and $\mu \equiv \mu(x,t)$ is the fluid dynamic viscosity. The third term on the right-hand side of Eq. (2) represents the contribution of the surface tension forces at the interface between fluids. The Dirac distribution function (δ_s) is used to indicate that the surface tension term is concentrated on that interface. Hence, σ is the surface tension coefficient, κ is the interface curvature and $\boldsymbol{n}$ is the normal to the liquid–gas interface.

A Bell-Collela-Glaz scheme [21] is used to estimate the velocity advection term of the Navier-Stokes equations. This scheme is stable for Courant-Friedrichs-Lewy (CFL) numbers smaller than one, which will be the case. In addition, a momentum-conserving formulation is used for this advection term.

As it is a two-phase flow problem [22], an interface capturing method must be used. Basilisk uses a VOF method, in which a liquid volume fraction $f(x,t)$ is defined to be able to differentiate the two fluids that take part in the problem. That volume fraction is $f = 1$ in fluid 1, considered as liquid, and $f = 0$ in fluid 2, considered as gas. Because of that, density and dynamic viscosity are locally defined as follows:

$$\rho(f) \equiv f\rho_1 + (1-f)\rho_2 \tag{4}$$

$$\mu(f) \equiv f\mu_1 + (1-f)\mu_2 \tag{5}$$

where ρ_1, ρ_2, μ_1 and μ_2 are the densities and dynamic viscosities of the first and second fluids, in this study fuel and air, respectively. By using the volume fraction variable, the advection equation for the density can

be replaced with an equivalent advection expression applied to this volume fraction:

$$\delta_t f + \nabla \cdot (fu) = 0 \tag{6}$$

This expression is used to compute the local value of f and, subsequently through Eq. (4) and Eq. (5), the local values of density and viscosity to eventually represent the interface between fuel and air.

Once that interface is captured, height functions are used to calculate the distance from the centre of each cell to the closest interface defined by a volume fraction field. Interface curvature is then computed estimating the derivatives of the height functions in each direction. Regarding surface tension, it is computed using a time-explicit scheme.

Spatial discretization is made by using a graded quadtree partitioning (for 2D problems) or octree (for 3D problems), the latter being the case of this study as it is a three-dimensional problem. A 2D example of this type of spatial discretization with its corresponding tree representation can be seen in Fig. 4 for visualization purposes.

Each finite volume generated is a cell. In 3D cases, each cell may be the *parent* of up to eight *children*. The root cell is the base of the tree and the level of a cell is defined by starting from zero for the root cell (full domain) and by adding one every time a group of eight descendant cells is generated. Thus, the code enables to set a maximum level of refinement for the entire simulation and some criteria to decide whether the mesh must be refined or not. This is the base of the AMR technique used by Basilisk, which generally implies to compute with a variable time step to keep a constant CFL number and ensure that CFL < 1, avoiding jeopardizing the stability of the previously described numerical methods. In these meshes, all the variables are collocated at the centre of each cubic discretization volume and are interpreted as the volume-averaged values. The use of this collocated definition makes momentum conservation simpler when dealing with mesh adaptation and is also necessary to use the Bell-Collela-Glaz scheme.

To finish this subsection, it is important to point out that Basilisk uses load balancing techniques to optimize the distribution of the discretized domain between processors and make computations and communications between them more efficient. More and detailed information about Basilisk code can be found visiting the code wiki and in the literature [20,21,23,24].

3.2. Operating condition

The fluid properties that define the operating condition to be studied here are detailed in Table 2. This operating condition is the one experimentally studied in [12,25] and numerically studied through LES simulations in [4], corresponding to injecting ambient-temperature fuel into an ambient-temperature and atmospheric-pressure chamber, so there is no fuel nor air pre-heating. These fuel properties can also be found in [26,27], as well as their variation with temperature and pressure, which may allow to get information to simulate other feasible operating conditions, giving reproducibility to this study.

Table 2
Fluid properties for the simulation's operating condition.

	Temperature [K]	ρ[kg/m^3]	μ[Pa·s]	σ[N/m]
Fuel (fluid 1)	298	681.7	$3.92\ 10^{-4}$	0.0197
Air (fluid 2)	298	1.185	$1.85\ 10^{-5}$	

A liquid fluid with the physical properties of n-Heptane is used as fuel, as it was the one used in the aforementioned works. As Basilisk will solve an incompressible two-phase problem, it needs to be provided with density ρ and dynamic viscosity μ of both fuel and air, as well as the surface tension σ between these two fluids.

This operating condition corresponds to an event of injection that gives rise to the velocity statistics shown in Table 3. These velocities were computed from planes normal to the discharge orifice in which solutions from the internal flow LES simulation carried out in [4] were recorded, as they are used as inflow boundary conditions for the DNS computed here (explained in detail in Subsection 4.2). For each plane, an azimuthal average is performed to obtain velocity profiles as a function of the nozzle radius, $u(r)$, and the same with the liquid volume fraction, $f(r)$. With the latter, the average liquid thickness of the plane can be obtained, and thus the velocities corresponding to the liquid fuel (where $f > 0$) and to the air (where $f = 0$). Finally, a temporal average is computed after getting data from all planes that are provided to the DNS simulation.

Radial and azimuthal velocities are of the order of magnitude of the axial one, a fact that makes possible the hollow-cone spray formation. Moreover, there are considerable velocity fluctuations that indicate that the injected flow is turbulent. As can be deducted by the air axial velocity mean value, part of the air is entering into the nozzle at the same time the fuel is being injected, as explained in Section 1.

Table 3
Averaged velocity statistics of fuel and air at the discharge orifice over the simulation time.

Velocity component	Fuel		Air	
	Mean	RMS	Mean	RMS
Axial [m/s]	16.82	15.85	−3.63	7.76
Radial [m/s]	14.67	13.80	3.26	5.14
Azimuthal [m/s]	7.11	6.68	1.53	2.38

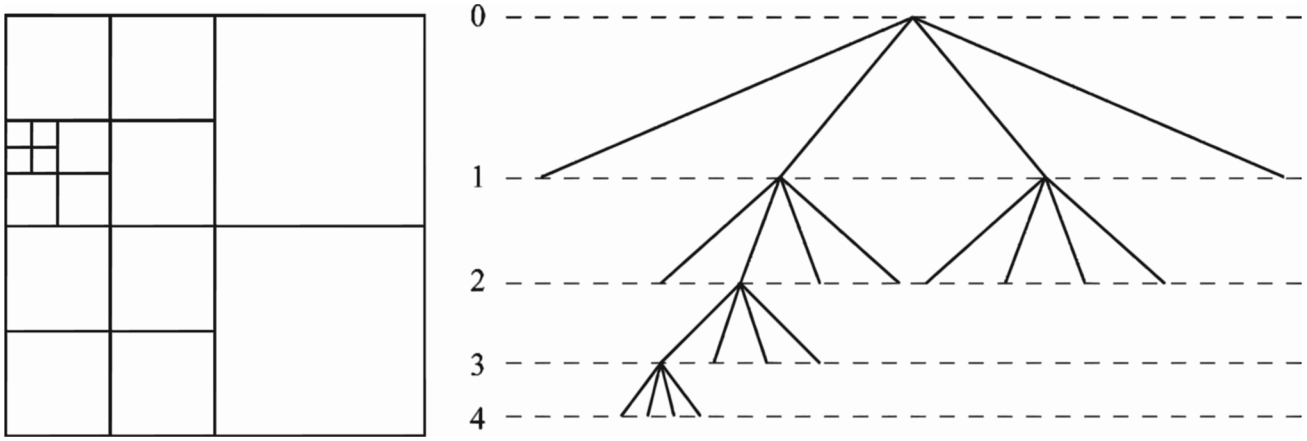

Fig. 4. Example of a 2D spatial discretization using a quadtree mesh (left) and its corresponding tree representation (right) [24].

4. External flow modelling

To be able to faithfully model the near field of the spray generated by the Danfoss pressure-swirl atomizer for the operating condition specified in the previous section and get a reliable behaviour of the injected liquid and its breakup, a good pre-processing work must be done. That includes selecting a mesh with a minimum cell size small enough to solve most of the turbulent scales, a proper computational domain, boundary conditions that represent well the surroundings of the problem and a realistic inflow condition for the fuel injected and the air that is being pulled inside the nozzle. All these topics are covered in the following subsections.

4.1. Numerical domain, mesh and boundary conditions

The choice of the domain, together with the type of mesh and its characteristics, turns out to be fundamental in terms of resolution achieved and computational effort needed, especially for DNS simulations. Due to Basilisk features and the spread angle of this kind of sprays, a cubic domain is the best option to choose. Regarding the mesh, a tree-structured cartesian mesh for 3D problems (*octree*) is used. This type of mesh will allow to use AMR techniques, as stated in Subsection 3.1 making possible to compute bigger domains (compared to uniform cartesian meshes) while keeping a high level of resolution. The main parameters of the simulation setup are detailed in Table 4.

The first decision to make is the minimum cell size, since it has to be small enough to resolve most of the energy scales up to the Kolmogorov scale η. For that reason, an estimation based on that scale's size is done in a similar way than in previous works [1,15], being $\eta\ LRe_{fuel}^{-3/4}$, with L a characteristic length, in this case the nozzle diameter D_0, and Re_{fuel} the Reynolds number of the liquid fuel taking into account the velocity magnitude in the nozzle, computed as explained in Subsection 3.2 and the fuel physical properties, having a value of $Re_{fuel} \approx 2200$. The result is $\eta \approx 0.95\mu m$, and thus the minimum cell size picked is $d_{x,min} = 1\mu m$. Although, as stated in [1], the common trend in the literature is to choose a minimum cell size twice the size of η respecting the criterion of $dx/\eta \leq 2.1$, here it is possible to choose a more approximate value thanks to the AMR.

As mesh refinement criteria are based on error thresholds, these must be defined to indicate the code where the mesh should be finer or coarser. Wherever the variation of the selected control parameters between neighbour cells is over the threshold values, the algorithm will apply the necessary refinements between iterations in those regions to reduce variations under the thresholds again. In this case, thresholds are set for the three velocity components u = (u,v,w), with a maximum variation value of 1 m/s each, and the liquid volume fraction f, with a maximum variation value of 1e-6. They were selected after testing some different options and watching how the mesh adapted to the injected liquid and its surroundings in a small domain. These values are strict enough to get a fine mesh in the liquid–air interaction areas, where vortices are produced, as can be seen in Fig. 5. That is the reason why the f threshold value is so small.

Once the minimum cell size and the refinement criteria are properly selected, the domain size must be defined. The goal is to simulate a domain as big as possible to have enough spray development to compare with previous studies and validate results, and for having enough droplets statistics to get reliable information about the droplet population generated in the primary atomization process. However, the domain size is limited by the computational resources available, so a balance was done testing different sizes to finally select a cubic domain of 8 mm side size. Nevertheless, this side size must be slightly increased, $l_{x,y,z} = 8.192$mm as can be seen in Table 4, due to the octree mesh and its way of working. Refinement levels represent powers of 2, since each refining step means reducing the initial cell by half. Thus, the level zero means that there would be only one cell (the full domain) and it would not be divided ($l_{x,y,z}/2 = l_{x,y,z}$), while the level ten means that the algorithm would perform ten divisions in a certain part of the mesh, reaching a minimum cell size of $l_{x,y,z}/2^{n_{ref}}$, which in that case would be $8.192/2^{10} = 8$ μm, as it was depicted in Fig. 4. According to this, to reach the desired minimum cell size of 1 μm in an 8 mm domain, thirteen levels of refinement are needed ($2^3 = 8192$) and thus the domain size has to be slightly increased to 8.192 mm to achieve exactly that 1 μm minimum cell size where necessary. Hence, both the domain size and the maximum refinement level $n_{ref,max}$ are defined through this reasoning.

CFL is the value of the Courant-Friedrichs-Lewy number, and it has been chosen based on previous works and smaller than one to ensure computation stability, as stated in Subsection 3.1. Having a fixed CFL number will lead to a variable time step dt mainly because of the changes in the mesh size performed by the AMR techniques. The parameter $n_{cells,0}$ indicates the number of cells of the cartesian uniform mesh used to discretize the domain at t = 0 μs, resulting in 256^3 16.78 millions of cells. This initial discretization and the choice of its number of cells is just based on having enough resolution to initialize the computation properly. In the first iteration of the simulation, the AMR algorithm will decide which zones of the mesh have to be refined and at which level, thus defining the resulting number of cells, similarly to the steps that can be seen in Fig. 5. Lastly, t_{simu} is the total simulated time, which is high enough to process resulting data in a stationary state, avoiding the spray's transient development.

It is important to highlight that Basilisk makes possible to refine the mesh permanently in certain zones of the domain. This feature is important for correctly feeding the inflow condition, as it is detailed in Subsection 4.2, and can be seen in the lower part of the mesh represented in Fig. 5.

In Fig. 6, a representation of the computational domain together with the atomizer's discharge orifice is shown.

Regarding boundary conditions, three different types are used: inflow, wall (blue) and outflow (green). In Fig. 6 it is possible to see where these different types of boundary conditions are applied to the domain. Inflow boundary condition is applied at the nozzle's discharge orifice and is mapped from the solution of an internal flow LES simulation. It consists of time-varying fields of velocity $u(t)$ and liquid volume fraction $f(t)$, while a Neumann boundary condition (value of the derivative is given) of zero-gradient is set for the pressure field p. A more detailed description of the inflow condition is presented in the next subsection. Wall boundary condition is applied to the face of the domain where the discharge orifice is located, and it is characterized by imposing a *no slip* condition to the velocity field, which equals to impose a Dirichlet boundary condition (value is given) of zero. Pressure has a Neumann zero-gradient condition at the wall as well and liquid volume fraction has a Dirichlet condition with a value of zero because, like velocity, it will be provided just at the nozzle exit through the inflow condition. Finally, the rest of the domain boundaries will have the outflow condition, since the generated droplets may leave the domain through any of those limits. This outflow condition will consist of Neumann conditions of zero-gradient for both the velocity and liquid volume fraction fields and a Dirichlet condition for the pressure field, setting an atmospheric-pressure value. A summary of the described boundary conditions can be found in Table 5, where **D** means Dirichlet and **N** means Neumann.

Table 4
Main simulation's setup parameters.

$l_{x,y,z}$ [mm]	$n_{ref,max}$ [-]	$d_{x,min}$ [μm]	$n_{cells,0}$ [-]	dt	CFL [-]	t_{simu} [μs]
8.192	13	1	256^3	variable	0.3	400

4.2. Mapped inflow condition

Prescribing realistic inflow boundary conditions is key for modelling

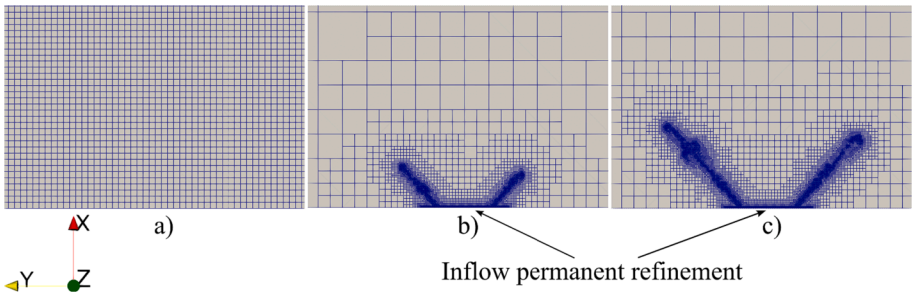

Fig. 5. Mesh representation at a centred plane normal to the Z axis. From left to right, snapshots at a) t = 0 μs, b) t = 5 μs and c) t = 10 μs.

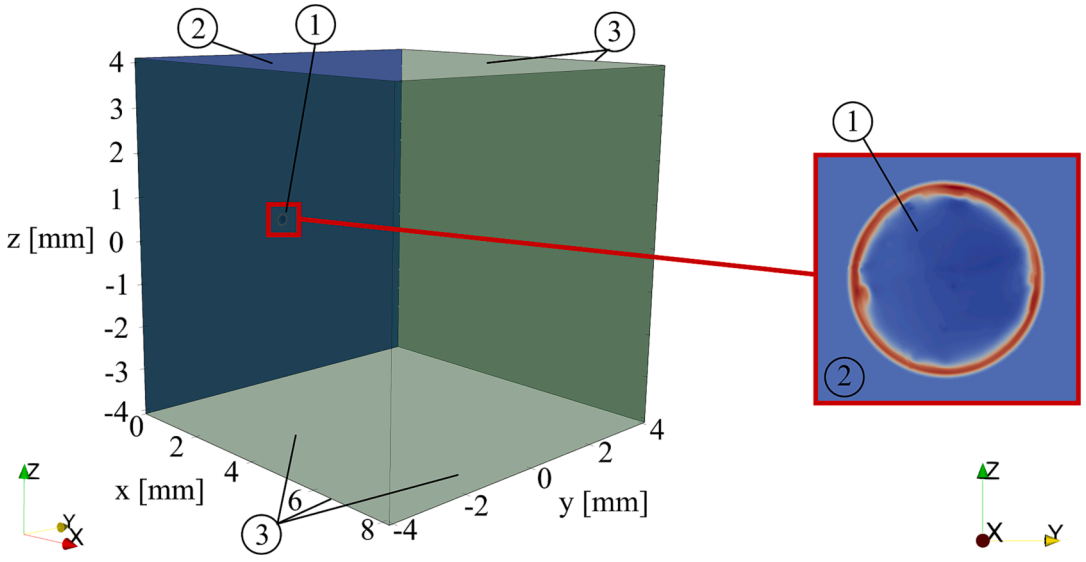

Fig. 6. Computational domain with a zoom of the discharge orifice placement. Numbers and colours denote the different boundary conditions applied.

Table 5
Boundary conditions applied to the simulation domain.

Variable	1. Inflow	2. Wall	3. Outflow
u	**D**: time-varying field	**D**: $u = 0$	**N**: zero-gradient
p	**N**: zero-gradient	**N**: zero-gradient	**D**: atmospheric pressure
f	**D**: time-varying field	**D**: $f = 0$	**N**: zero-gradient

the first stage of the external flow and may significantly enhance the level of prediction of the primary atomization phenomenon, as concluded in [16]. Being able to capture the instabilities of the liquid film when leaving the nozzle leads to a better comprehension of how the very first breakup is triggered. In that regard, solutions from internal flow simulations can provide the level of detail necessary for these purposes better than any synthetic boundary condition, both in terms of information about turbulence and of the behaviour of the liquid film with time.

For that reason, results from the LES internal flow simulation of the Danfoss atomizer carried out in [4] with the open-source code OpenFoam are used here as inflow boundary conditions. Every 50 ns, velocity and liquid volume fraction fields are recorded in a plane located at the discharge orifice itself and normal to the injection axis, as depicted in Fig. 7. That recording frequency is high enough, as it has been checked that 50 ns are way below the air core rotation period.

These results are then interpolated to the mesh that is going to be used with Basilisk and here is where the feature of refining permanently some areas of the domain, mentioned in Subsection 4.1, takes importance. To have a detailed inflow condition throughout the whole simulation, instructions are given to Basilisk to refine the mesh at the discharge orifice and its surroundings permanently with the minimum cell size (1 μm), having a constant-size mesh at this area. This way, results of u and f contained in the planes extracted from the LES simulation are interpolated from the LES mesh into a uniform cartesian mesh of 1 μm covering the discharge orifice. Once interpolated, values are provided to Basilisk, that reads and collocates them in its own mesh which, thanks to the permanent refining, will have the same one-micrometre-size at the discharge orifice. Fig. 8 shows, for a specific time t, a comparison between the velocity and liquid volume fraction planes extracted from the LES simulation and the same planes already mapped and used by Basilisk in the DNS simulation. As depicted in that figure, there is a good level of agreement between the LES solutions and the mapped fields, fact that will be reaffirmed when validating results in Section 5.

As can be seen, most of the air in the nozzle plane (represented in blue in the bottom planes) has negative axial velocities, which means is being drawn inside the nozzle by the pressure drop generated by the internal flow dynamics already explained in Section 1.

In Fig. 9, three different temporal instants of the mapped inflow conditions are represented in order to see how they vary with time. As it can be seen, the DNS simulation has been fed with a detailed inflow condition directly extracted from the internal flow modelling, taking into account turbulence through the velocity field variations and also the variability of the liquid film thickness that this atomizer's way of working produces. This will make possible to capture instabilities when fuel is injected and hence the primary atomization mechanisms, as it will be seen in Section 5.

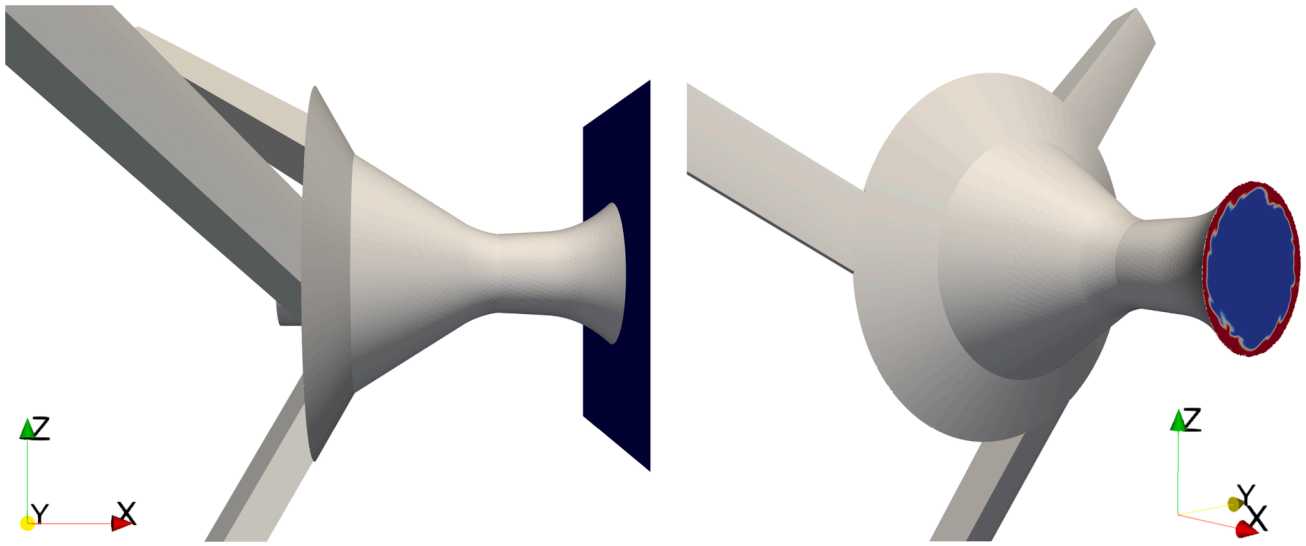

Fig. 7. Plane in which results from the LES internal flow simulation are recorded.

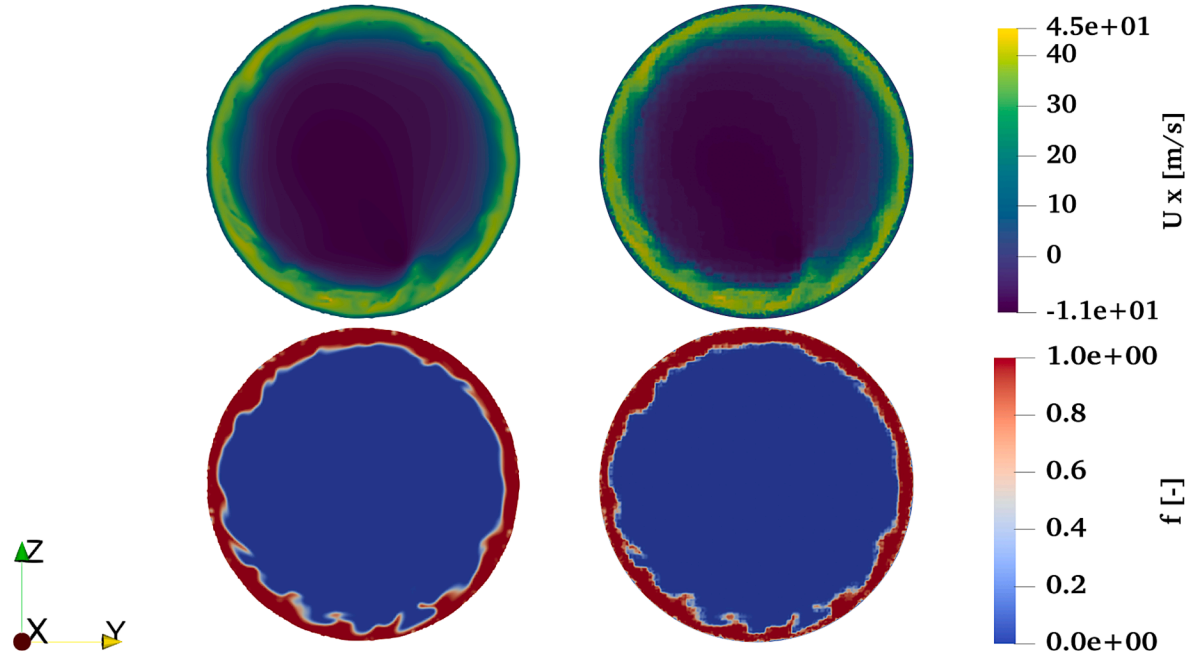

Fig. 8. Comparison between LES planes (left column) and mapped planes used by Basilisk (right column) for the axial velocity (top row) and liquid volume fraction (bottom row) fields.

5. Results

5.1. Spray shape and development

First, some qualitative results will be shown in terms of development and shape of the spray produced when simulating by means of high-resolution DNS the injection condition described in Subsection 3.2. All the figures showing qualitative results have been extracted using Paraview, the open-source application for visualization [28].

Fig. 10 shows the temporal evolution of the liquid fuel being injected into the ambient air and, hence, the spray development. For convenience, the spray development has only been represented until $t = 100$ μs, as it is the time when the spray starts to leave the domain, so its shape suffers no macroscopic changes from then.

As can be seen, the fuel is exiting the nozzle directly with the hollow-cone shape. This is because the internal flow solutions mapped and used as inflow conditions are already developed, meaning that the air core inside the nozzle is already formed and the liquid film has the appropriate behaviour in terms of thickness and velocity variability at the nozzle exit to give rise to that spray shape.

5.2. Validation

To be able to fulfil the main objective of this study, it is important to validate the results obtained from the simulation. To that end, both qualitative and quantitative DNS results are compared here with experimental and previous numerical results.

In [12], Miglierina studied the shape and some characteristics of the external flow produced by a pressure-swirl atomizer in a laboratory context for the same operating condition and geometry studied here,

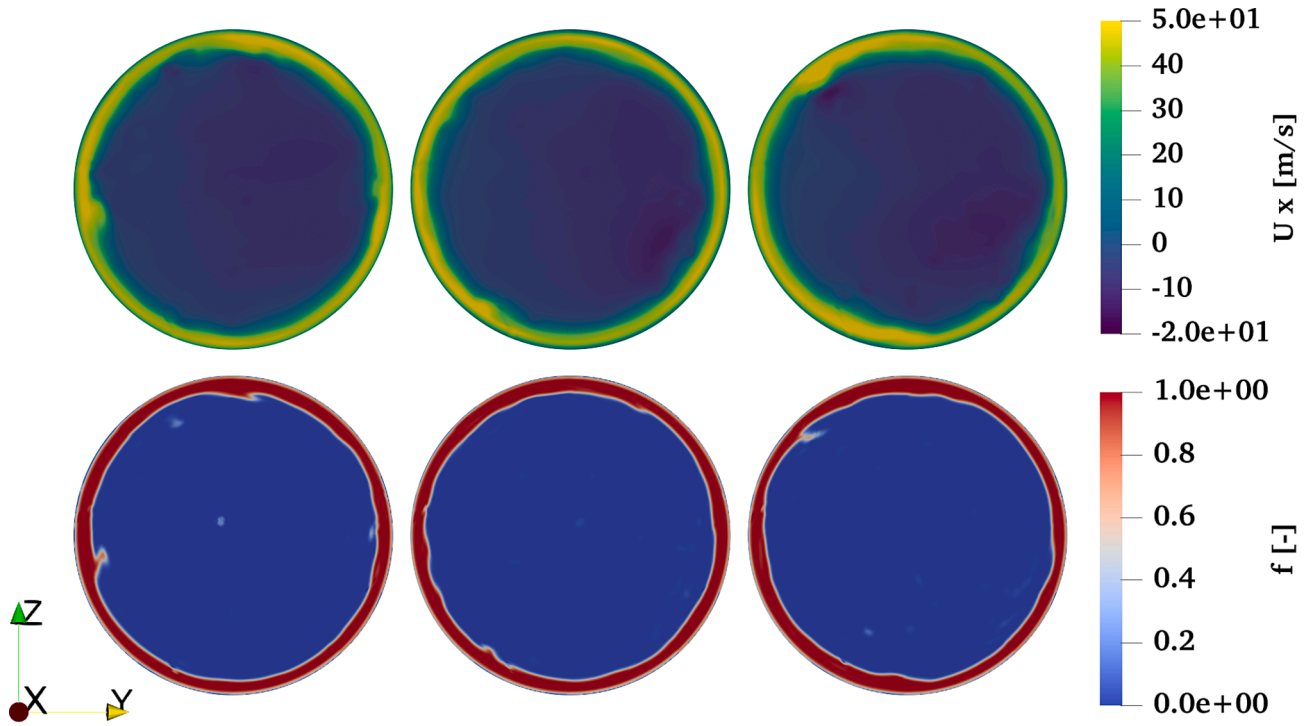

Fig. 9. Temporal evolution of the mapped axial velocity (top row) and volume fraction field (bottom row) inflow conditions. From left to right column, snapshots at t = 5 μs, t = 10 μs and t = 15 μs.

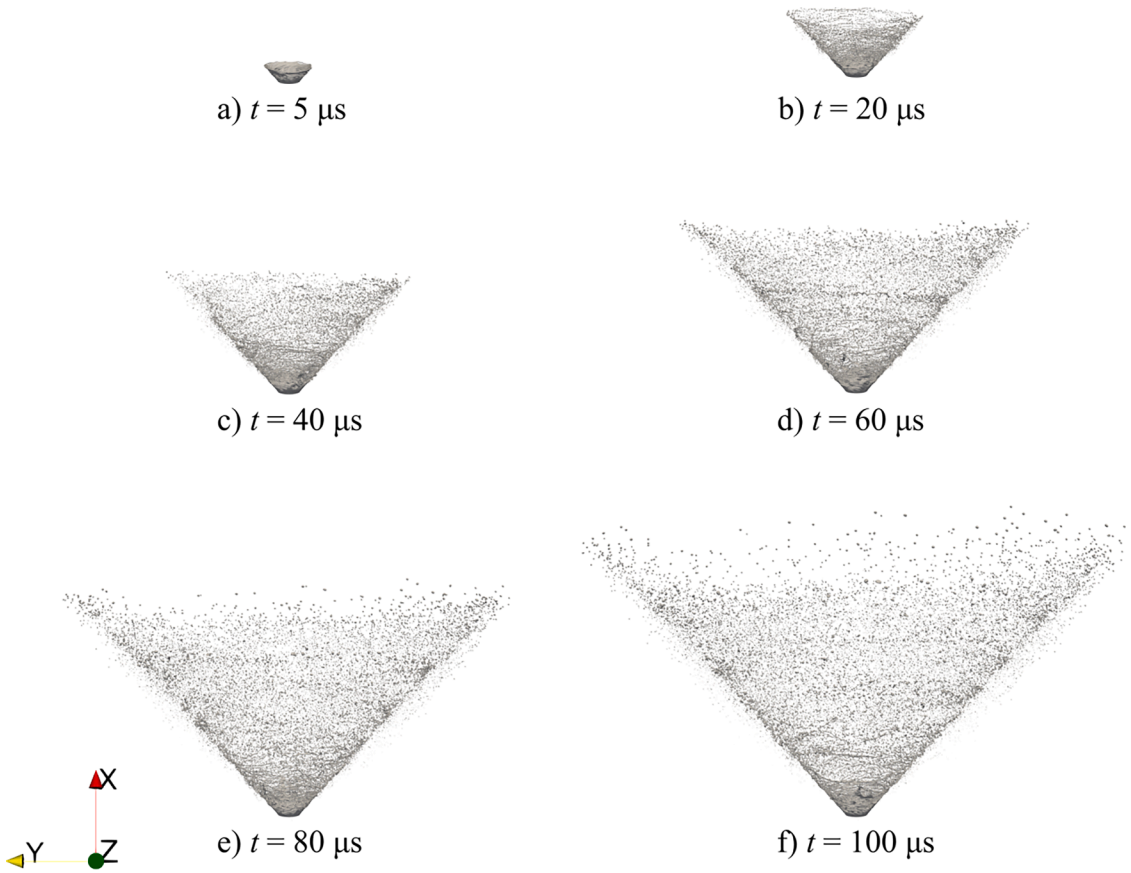

Fig. 10. Spray development. Snapshots of the liquid volume fraction contour *iso*-surface (α = 0.5).

using microscopic shadowgraphy to that end. After measuring, he developed some post-processing techniques to extract information from the photographs taken. Specifically, the spray contour length and the average drop diameter were computed. Then, he compared his results with previous experimental and LES ones, finding noticeable differences between them (droplet average diameter much bigger than that of the experimental and LES works), mainly due to his post-processing techniques were novel and not enough developed. Nevertheless, the visualization techniques he used allowed him to get spray pictures way better and clearer than the ones available until then and, because of that, one of those pictures is used here to validate the shape of the spray computed through DNS modelling. From a qualitative point of view, in Fig. 11 an experimental picture taken by Miglierina [12] is compared with the 3D contour (iso-surface for $\alpha = 0.5$) of the DNS simulation spray for $t = 100$ μs. The half of the spray's spread angle θ is also represented.

This comparison shows the good agreement that exists between the experimental picture and the DNS-modelled spray both in terms of droplets macroscopic distribution and spray's spread angle. Both sprays show a dense liquid area until reaching the first millimetre in the axial direction (X axis). In the first 0.5 mm, the fuel sheet keeps mostly intact, while, from that axial distance, it starts breaking mainly into ligaments, as was also observed by Shao et. al in [16]. It is in those first 0.5 mm where the liquid film instabilities that promote the primary atomization, represented in the zoom made in the above figure, are clearly visible. This fact confirms that the information mapped from the LES solutions is well developed in terms of turbulence and liquid thickness variation and that the mesh resolution used in the DNS simulation is high enough to catch those instabilities, and thus to predict the liquid breakup.

After the first millimetre, most of the ligaments have broken into small droplets, leading to a less dense zone. Finally, after 2 mm axial distance, it is possible to see that droplets with slightly bigger size are being formed, both in the experimental and computational sprays, maybe due to some early coalescence phenomena. This trend will be better explained when analysing the droplet population in Subsection 5.3.

Regarding quantitative validation, on the one hand, the Swirl Number (SN) has been computed from DNS results at several planes normal to the injection axis located at the nozzle ($x = 0$ μm) and at three different axial positions downstream ($x = 100$ μm, $x = 200$ μm and $\times = 300$ μm). It has been computed for each microsecond of simulated time and then a temporal average has been performed. This way, SN results can be compared to those obtained in [4] for the LES simulation.

The SN represents the relationship between the swirling momentum and the axial motion, and can be expressed as follows:

$$SN = \frac{G_{tg}}{RG_{ax}} = \frac{\int_0^R wur^2 dr}{R\int_0^R u^2 dr} \tag{7}$$

where G_{tg} is the flow rate of the tangential momentum's axial component over the axial cross-section, G_{ax} is the flow rate of the axial momentum's axial component across the axial cross-section, R is the nozzle's outer radius and w and u are the corresponding tangential and axial velocities at a radial position r, respectively.

The axial evolution of the SN for the first 300 μm of the DNS spray is depicted in Fig. 12, together with the axial evolution of the SN obtained in [4] after carrying out both the internal and external LES simulations. Negative axial coordinates represent the inner part of the injector.

It is clearly visible that the Swirl Number values computed from DNS solutions are in good agreement with those of LES simulations, which means that the swirling motion is well recovered after mapping the LES solutions and using them as inflow conditions, both in the nozzle itself and in the liquid injected downstream. These results ensure the validity

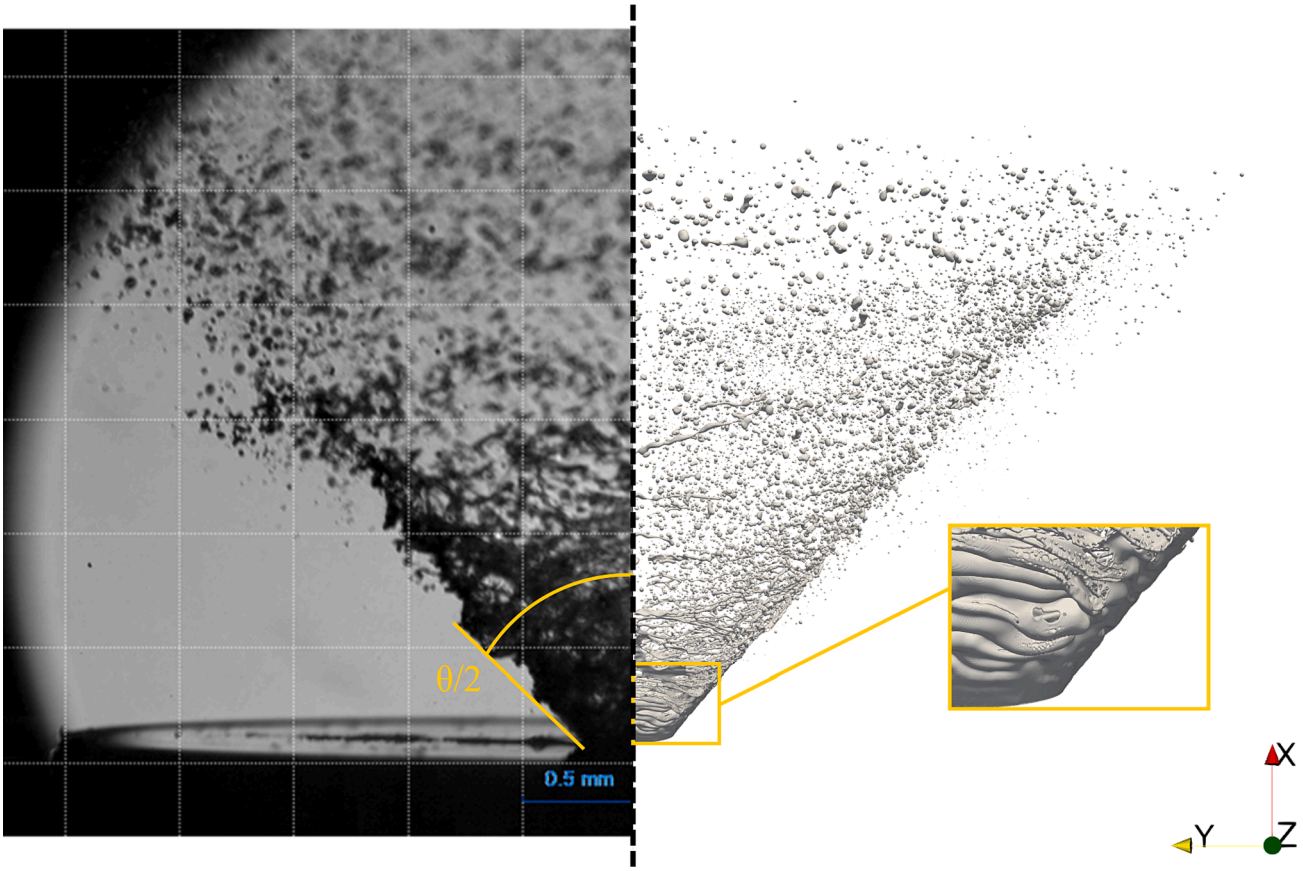

Fig. 11. Comparison of the DNS spray at t = 100 μs with an experimental image taken by Miglierina [12]. The zooming part represents the first stage of the spray before the liquid breakup, where fuel instabilities are visible.

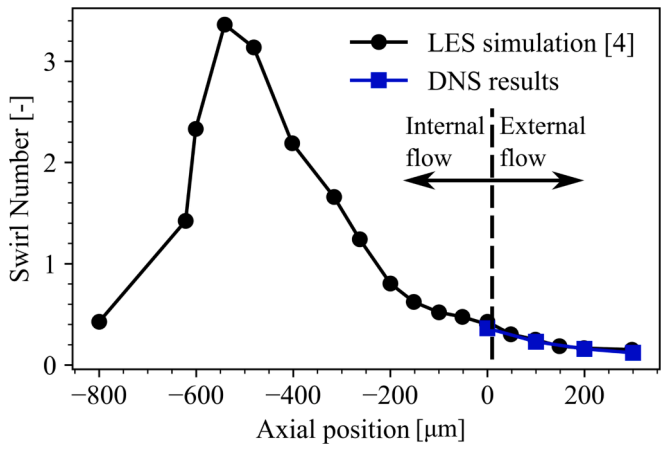

Fig. 12. Comparison of the axial evolution of the Swirl Number between the LES simulation (internal + external flow) and the DNS simulation (only external flow).

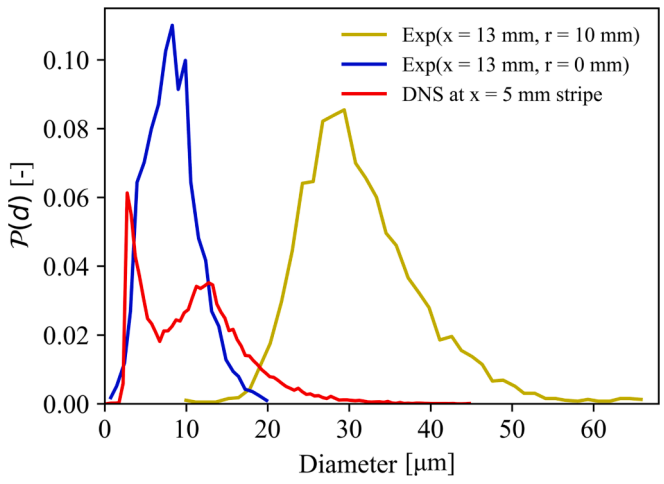

Fig. 13. Droplet sizes distribution PDFs. Blue. experimental data at x = 13 mm and r = 0 mm; yellow. experimental data at x = 13 mm and r = 10 mm; red. numerical results at x = 5 mm stripe normal to the injection axis.

of the mapping process and, to some extent, of the DNS simulation, as information is well recovered without important losses.

On the other hand, and following with the quantitative results comparison, the spray's spread angle θ has been computed from the DNS results to compare the value obtained from the simulation with the nominal value given by Danfoss [19]. The angle was computed detecting liquid through the volume fraction variable f in planes normal to the injection axis (Y-Z planes) each 10 μm from the nozzle until reaching 400 μm in the axial direction for several temporal solutions, so a temporal average with its standard deviation was computed. In Table 6, the comparison between the spray's spread angle got from the DNS simulation and the nominal value for this specific atomizer is shown.

The fact of having an error smaller than 3 % demonstrates that the spray shape is realistic and, in general, macroscopic characteristics are well predicted by the DNS simulation, as it could also be seen in the spray morphology comparison with experiments done in Fig. 11.

Additional quantitative results validation related to droplets distribution will be done in the next subsection for convenience and coherent order of the paper.

5.3. Droplets distribution

Now that the DNS simulation has been validated through a series of results that match properly with experimental measurements and nominal features of the atomizer, results regarding droplet characteristics are presented here. The main idea is to analyse the droplet population generated by the primary atomization phenomenon by extracting the characteristic droplet sizes and how these droplets are distributed spatially across the computational domain. That information will give some ideas of how primary atomization is taking place in this specific case.

First, and to give more reliability to the following results, a Probability Density Function (PDF) of the droplet sizes distribution extracted from the DNS results is compared with experimentally-measured-data PDFs [4] in Fig. 13. The available experimental distributions were computed after measuring droplets through PDA at an axial position of $x = 13$ mm away from the nozzle's discharge orifice and in two different radial positions; injection axis ($r = 0$ mm) and $r = 10$ mm, which is the radial position where the injected fuel should be following the nominal spray's spread angle. The DNS distribution was computed at the furthest axial position possible, considering the computational domain used, in order to have results as close as possible to the experimental ones to make the comparison. That position is around $x = 5$ mm because, although the domain has approximately 8 mm axial length, the injected liquid leaves the domain shortly after 5 mm axial distance due to the spread angle of the hollow-cone spray. To get a significant sample of droplets to compute statistics, not only a plane at $x = 5$ mm but a stripe of 100 μm width centred at $x = 5$ mm was considered as control volume to collect droplets data. Besides, for all the distributions shown in this subsection, the time considered to average data and compute statistics was 100 μs $< t <$ 400 μs, because, as stated in Subsection 5.1, it is at approximately $t = 100$ μs when the spray starts to go out of the domain and that moment was considered as the end of the spray's transient phase.

Table 6
Comparison of the spread angle value between nominal and DNS results.

	Nominal value	DNS simulation	Error
Spread angle θ	80°	82.3° ± 0.6°	2.875 %

Considering experimental PDFs, it can be seen that when data is collected near the injection axis (blue line) is more probable to find small droplets from 2 to 18 μm with a peak around 10 μm, while when data is collected away from the injection axis (yellow line) there is no probability of finding small droplets but bigger droplets between 18 μm and 54 μm with a peak around 30 μm. From the numerical standpoint, the PDF computed from DNS results shows two main peaks: one located between 2 μm and 4 μm and the second one located between 10 μm and 14 μm, being higher the probability of finding small droplets.

A statistical comparison has been carried out, computing averaged droplet diameters and their standard deviation for both experimental (from the distribution plot in Fig. 13) and numerical (from the droplet population in the aforementioned control volume) data. Experimental data measured in the injection axis has a mean diameter of 8.3 μm with a standard deviation of 3.2 μm, while data measured at r = 10 mm presents a mean diameter of 31.4 μm with a deviation of 7.6 μm. DNS data shows an average droplet diameter of 13.6 μm with a deviation of 4.7 μm. As can be seen, DNS results are more like the experimental ones in the injection axis, as they are computed much closer to the breakup region and, as it happens in the experimental measurements in r = 0 mm, small droplets are predominant. Besides, deviations are smaller for those measurements compared to that of the experimental data in r = 10 mm, which means that droplet size variability is higher when going further from the nozzle.

The differences observed in probability values (Y axis) are mainly because experimental distributions are measured in two different control volumes for the same axial distance (because of the PDA working principle), so two different PDFs have been represented instead of just one like for the DNS data. Measurement uncertainties may also have a

certain influence in the results, but cannot be quantified here since the authors do not have the necessary data.

Despite the differences, some important common trends can be observed between experimental and numerical data. As it happens with experimental results, the numerical PDF indicates that there are mainly two different characteristic ranges of droplet sizes at the same axial distance, coexisting smaller and bigger droplets but with more probability of finding the smallest range of sizes. Moreover, the ratio between the peak diameters (peak locations in the X axis) are similar between experimental and numerical data, being between 3 and 4 in both cases (big droplets are between 3 and 4 times bigger than the small ones), indicating that the relationship between characteristic sizes recovered by the DNS is also representative of a real breakup process. Hence, both kind of results (experimental and numerical) are totally consistent and somewhat show a compatible behaviour.

However, characteristic sizes shown by the distribution computed from DNS data are significantly smaller than those of the experimental results. That is because data from simulation is collected closer to the discharge orifice, and thus closer to the primary atomization region, where liquid starts to breakup in ligaments and then in small droplets, as depicted in Fig. 10 and Fig. 11. By the trends in the PDFs, it is expected that, the more the distance to the nozzle, the bigger the droplets, probably due to coalescence phenomena. This assumption can be justified looking at Fig. 14, where some PDFs of sizes distributions are plotted depending on the axial stripe where data is collected. Note that for those distributions, the domain is just filtered axially but not in Y and Z directions, so all radial distances are considered.

Each PDF has been computed collecting droplets data in an axial range of 1 mm from $x = 0$ to $x = 5$ mm, which is feasible since droplets' positions are known. As can be seen, the coalescence trend is confirmed in this figure, since the distribution changes as the axial distance increases, losing probability of finding small droplets and gaining probability of finding bigger ones. Furthermore, the bigger the axial distance considered, the more to the right is located the peak that represents the biggest sizes, fact that confirms that there is a coalescence phenomenon consisting of collisions between droplets which result is the generation of big droplets from several smaller ones. The only region where this trend does not hold is at $0 < x < 2$ mm. The distribution of the $1 < x < 2$ mm stripe shows more probability of finding small droplets and less of finding big ones than that of the $0 < x < 1$ mm stripe. That makes sense, since is between 0 and 1 mm where the primary breakup is happening, as seen in Fig. 11, and small droplets are still emerging from ligaments and from the injected liquid film itself. That breakup is totally done by the time the injected spray arrives to the $1 < x < 2$ mm stripe, and that is why in this area is more possible to find smaller droplets. From there, sizes start to increase as the measuring control volume moves away in the axial direction, especially after $x = 3$ mm.

Apart from the axial study, the same analysis but considering radial distances (Y and Z distances simultaneously) instead has been performed in order to see where small and big droplets are more probable to be found. Now, the domain is not filtered in the axial direction so, for each Y and Z distance considered, droplets at all axial distances are taken into account. This is shown in Fig. 15.

Looking at that figure, it is easy to see that the radial study shows exactly the same trend than that of the axial one. Again, the probability of finding bigger droplets is higher when the radial distance increases, while finding smaller droplets is less probable following that same radial-increasing path.

These results confirm that big droplets are most likely to be found at regions far from the nozzle and far from the injection axis, following the trajectory marked by the spray's spread angle, and that the characteristic size of the droplets increases as it does the distance to the nozzle. Small droplets are concentrated close to the nozzle, where the primary breakup happens, and near the injection axis when axial distance increases. Those trends are the same than that of the experimental measurements and their processed results, as depicted in Fig. 13.

To give a general perspective about the characteristic size of the droplet population produced by the DNS-modelled external flow, the PDF of the droplet sizes distribution considering the full computational domain is presented in Fig. 16.

As shown in the above figure, there is a clear predominance of small droplets over big ones as expected, since only the very near field has been computed and analysed through DNS and it is in that region where primary atomization is taking place. The black-dashed line represents the droplet size lower limit, which is $d = 2$ μm. Droplets which size is below two times the minimum cell size are not considered as they may not be well captured by the code due to the mesh resolution used. Only with higher resolutions, and hence a higher computational effort that may do the task unfeasible, would be possible to see if smaller droplets are being generated in the process. From the big sizes standpoint, results show that is difficult to find droplets bigger than 25 μm. The mean droplet diameter in the whole computing domain is 8.5 μm with a standard deviation of 0.5 μm. These near-field results help to highlight the considerable differences that exist in the obtained characteristic sizes depending on where data is collected, especially if this distribution is compared with the far-field results provided by the experimental measurements shown in Fig. 13. These differences reflect the importance of studying not only the far-field behaviour but also what is happening in the first millimetres of the spray due to the key role that these near-field behaviour has in the development of the spray downstream.

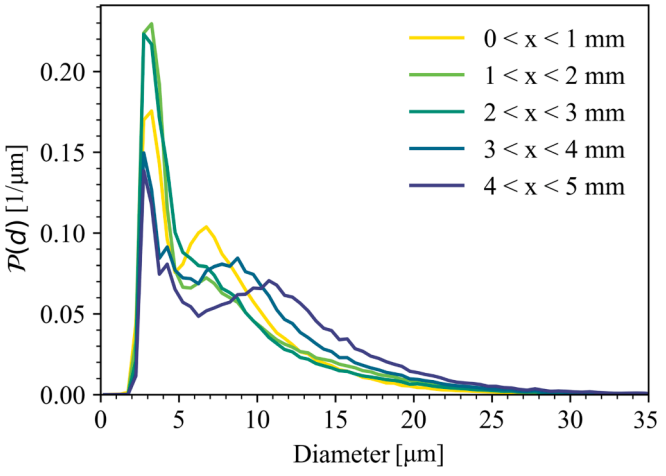

Fig. 14. Droplet sizes distributions PDFs considering different axial stripes from the nozzle exit (x = 0 mm) to x = 5 mm.

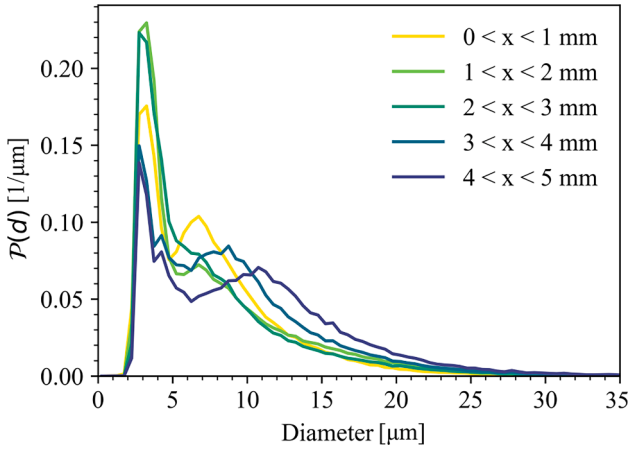

Fig. 15. Droplet sizes distributions PDFs considering different radial stripes from the injection axis (r = 0 mm) to the end of the domain (r = 4 mm).

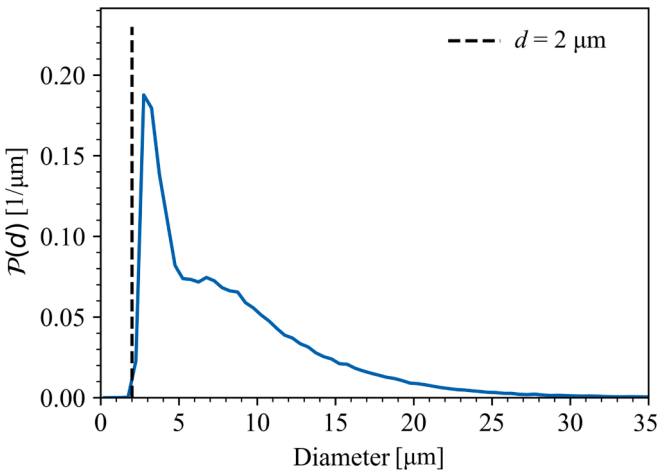

Fig. 16. Droplet sizes distribution PDF for the full computational domain.

The results shown here enforce the necessity and relevance of performing numerical studies in the general investigation process of these kind of problems and the important amount of information that they are able to provide, enhancing substantially the comprehension of what is observed experimentally downstream.

6. Conclusions

Throughout this paper, an analysis of the external flow produced by a simplex pressure-swirl atomizer in an injection condition representative of an academic burner that replicates characteristic phenomena of aeronautical gas turbine's combustion chambers has been carried out. Specifically, the droplet population generated in the primary atomization process taking place when injecting n-Heptane into atmospheric air with a Danfoss atomizer has been studied.

This study has been conducted by means of a high-fidelity DNS simulation, highlighting the main stages of the process. Pre-processing tasks were done, consisting of knowing the relevant atomizer's geometry features and its way of working to subsequently configure an appropriate computational domain and an AMR octree-type mesh with a resolution high enough to solve most of the energy scales and capture the breakup process. Besides, fuel and air properties were necessary to simulate accurately the intended injection condition. Boundary conditions were then set, having a special relevance the inflow ones, which were extracted and interpolated from a previously done internal-flow LES simulation. Mapping these solutions provided time-varying velocity and volume fraction fields that made possible to faithfully represent the turbulence and instabilities in both phases (fuel and air) at the discharge orifice and to have a realistic injection event. After computations were finished, post-processing tasks were carried out to get all the necessary quantitative and qualitative data to validate the obtained results and contribute with interesting droplet population ones.

From the DNS simulation, some injector's nominal features and characteristics observed in experiments were well recovered. The spread angle of the DNS spray presented an error smaller than 3 % compared with the nozzle's nominal value (given by the manufacturer). Furthermore, the experimental and DNS spray's macroscopic shapes were alike, presenting a similar dense liquid area and droplets and ligaments arrangement. It was also demonstrated the validity of the inflow boundary conditions mapping process by computing the Swirl Number, since values obtained at different axial distances were almost equal to those obtained in the LES simulation.

The droplet population results, also validated by comparing the droplet sizes PDF at the furthest axial position possible for the computational domain used with some experimental ones, provided helpful results to comprehend how the atomization process is taking place. On the one hand, it was observed that small droplets predominate over big ones as it was expected, since just the very-near field was modelled and primary atomization was well captured. Moreover, in a stationary situation, the injected fuel was fully broken into ligaments and droplets within the first millimetre in the axial direction, so an early atomization is achieved thanks to the instabilities of the liquid film injected in the shape of a swirling hollow-cone spray. On the other hand, coalescence phenomena were observed as the axial and radial distances increase, growing the possibilities of finding bigger droplets and decreasing the possibilities of finding smaller ones as the distance to the nozzle and to the injection axis increases. This way, small droplets were concentrated in the primary breakup region and near the injection axis when moving away in the axial direction. All these results were also visible when comparing the experimental and the DNS sprays.

The aforementioned results show clearly the important differences in characteristic ranges of sizes that exist depending on where data is collected. That is clearly visible when comparing numerical and experimental results, being bigger the droplets of the experimental study. This fact reinforces the idea of the coalescence phenomena already observed in the first 5 mm of the DNS spray, since experimental data is collected way downstream numerical data. That highlights the importance of studying not only experimental results, which may give good information about the far-field situation of the spray, but also perform numerical simulations of the near-field behaviour, since the latter has a huge influence over the spray development and thus cannot be disregarded. Besides, this kind of statistical results can be used to develop a phenomenological model able to predict how atomization is going to be depending on the fuel injected or the operating condition, a model that could be then implemented in lower-resolution RANS and LES codes to give them the capability of modelling atomization as accurate as possible. For that reason, in the future, works focused on simulating different fuels and injection conditions are intended to be done, now that the DNS modelling is validated. Combining these two factors, a series of simulations can be planned to get results when varying the governing non-dimensional numbers (Reynolds and Weber) and then it would be possible to study their influence on the droplet population in an isolated way. Those results would allow to develop the phenomenological model. This work demonstrates that a good prediction of that early injection stage can be done, obtaining common trends with experimental observation, and that achieving a good synergy between numerical and experimental results in this kind of problems leads to a better comprehension of the atomization process.

CRediT authorship contribution statement

F.J. Salvador: Conceptualization, Formal analysis, Investigation, Methodology, Project administration, Supervision; Writing – review & editing. **P. Martí-Aldaraví:** Conceptualization, Formal analysis, Investigation, Methodology, Supervision, Writing – review & editing. **A. Lozano:** Conceptualization; Data curation, Formal analysis, Investigation, Methodology, Validation, Writing – original draft. **H. Taghavifar:** Formal Analysis, Writing – review & editing. **A. Nemati:** Formal Analysis, Writing – review & editing.

Declaration of Competing Interest

The authors declare that they have no known competing financial interests or personal relationships that could have appeared to influence the work reported in this paper.

Data availability

Data will be made available on request.

Acknowledgements

This research has been funded by the Spanish "Ministerio de Ciencia e Innovación" through the project TED2021-129719B-C22: "Micromixes utilization for stable continuous hydrogen combustion for zero-carbon aviation" MIXSHY, belonging to the program "Programa de proyectos estratégicos de transición ecológica y digital". The authors thankfully acknowledge the computer resources at MareNostrum and the technical support provided by Barcelona Supercomputing Center (RES-IM-2022-2-0018). Lozano A. is supported through the contract FPU21/02749 of the "Ministerio de Educación y Formación Profesional".

References

[1] Crialesi-Esposito M, Gonzalez-Montero LA, Salvador FJ. Effects of isotropic and anisotropic turbulent structures over spray atomization in the near field. Int J Multiph Flow 2020;150(December):2022. https://doi.org/10.1016/j.ijmultiphaseflow.2021.103891.
[2] Payri R, Salvador FJ, Carreres M, Moreno-Montagud C. A computational methodology to account for the liquid film thickness evolution in Direct Numerical Simulation of prefilming airblast atomization. Int J Multiph Flow 2023;161 (September 2022). https://doi.org/10.1016/j.ijmultiphaseflow.2023.104403.
[3] Mongia H. TAPS: a fourth generation propulsion combustor technology for low emissions. In: AIAA international air and space symposium and exposition: the next 100 years; Jul. 2003, no. July. p. 1–11, 10.2514/6.2003-2657.
[4] Ferrando D, et al. Modelling internal flow and primary atomization in a simplex pressure-swirl atomizer. At Sprays 2022;33(3):1–28. https://doi.org/10.1615/atomizspr.2022044824.
[5] Amini G. Liquid flow in a simplex swirl nozzle. Int J Multiph Flow 2016;79:225–35. https://doi.org/10.1016/j.ijmultiphaseflow.2015.09.004.
[6] Park BS, Kim HY, Yoon SS. Transitional instability of a pressure-swirl atomizer due to air-core eruption at low temperature. At Sprays 2007;17(6):551–68. https://doi.org/10.1615/atomizspr.v17.i6.40.
[7] Nouri-Borujerdi A, Kebriaee A. Numerical simulation of laminar and turbulent two-phase flow in pressure-swirl atomizers. AIAA J 2012;50(10):2091–101. https://doi.org/10.2514/1.J051331.
[8] Liu C, Liu F, Yang J, Mu Y, Hu C, Xu G. Experimental investigations of spray generated by a pressure swirl atomizer. J Energy Inst 2019;92(2):210–21. https://doi.org/10.1016/j.joei.2018.01.014.
[9] Dafsari RA, Lee HJ, Han J, Park DC, Lee J. Viscosity effect on the pressure swirl atomization of an alternative aviation fuel. Fuel 2019;240:179–91. https://doi.org/10.1016/j.fuel.2018.11.132.
[10] Laurila E, et al. Computational and experimental investigation of a swirl nozzle for viscous fluids. Int J Multiph Flow 2020;128. https://doi.org/10.1016/j.ijmultiphaseflow.2020.103278.
[11] Durdina L, Jedelsky J, Jicha M. Investigation and comparison of spray characteristics of pressure-swirl atomizers for a small-sized aircraft turbine engine. Int J Heat Mass Transf 2014;78:892–900. https://doi.org/10.1016/j.ijheatmasstransfer.2014.07.066.
[12] Miglierina L. Liquid injection for gas turbine. Rouen 2021.
[13] Alajbegovic A, Meister G, Greif D, Basara B. Three phase cavitating flows in high-pressure swirl injectors. Exp Therm Fluid Sci 2002;26:677–81. https://doi.org/10.1016/S0894-1777(02)00179-6.
[14] Laurila E, Roenby J, Maakala V, Peltonen P, Kahila H, Vuorinen V. Analysis of viscous fluid flow in a pressure-swirl atomizer using large-eddy simulation. Int J Multiph Flow 2019;113:371–88. https://doi.org/10.1016/j.ijmultiphaseflow.2018.10.008.
[15] Galbiati C, Tonini S, Weigand B, Cossali GE. Direct numerical simulation of primary break-up in swirling liquid jets; 2016.
[16] Shao C, Luo K, Yang Y, Fan J. Detailed numerical simulation of swirling primary atomization using a mass conservative level set method. Int J Multiph Flow 2017;89:57–68. https://doi.org/10.1016/j.ijmultiphaseflow.2016.10.010.
[17] T. C. of S. Workshops. http://www.tcs-workshop.org.
[18] Vegad CS et al. Experimental study of near field regions of n-heptane spray. In: 31th Conf. Liq. At. Spray Syst. 6-8 Sept. 2022, no. September. p. 6–8; 2022.
[19] Danfoss OD-H product website." https://store.danfoss.com/en/Climate-Solutions-for-%0A661heating/Burner-components/Oil-nozzles/Oil-Nozzles%2C-OD-H%2C-0-35-gal-%0A662h%2C-1-35-kg-h%2C-80-°%2C-Hollow/p/030H8103.
[20] De Vita F, et al. Basilisk code; 2014. http://basilisk.fr/.
[21] Bell JB, Colella P, Glaz HM. A second-order projection method for the incompressible Navier-Stokes equations. J Comput Phys 1989;85(2):257–83.
[22] Salvador FJ, Hoyas S, Novella R, Martínez-López J. Numerical simulation and extended validation of two-phase compressible flow in diesel injector nozzles. Proc Inst Mech Eng Part D J Automob Eng 2011;225(4):545–63. https://doi.org/10.1177/09544070JAUTO1569.
[23] Popinet S. An accurate adaptive solver for surface-tension-driven interfacial flows. J Comput Phys 2009;228(16):5838–66. https://doi.org/10.1016/j.jcp.2009.04.042.
[24] Popinet S. Gerris: a tree-based adaptive solver for the incompressible Euler equations in complex geometries. J Comput Phys 2003;190(2):572–600. https://doi.org/10.1016/S0021-9991(03)00298-5.
[25] Verdier A, Marrero Santiago J, Vandel A, Saengkaew S, Cabot G, Grehan G, et al. Experimental study of local flame structures and fuel droplet properties of a spray jet flame. Proc Combust Inst 2017;36(2):2595–602.
[26] NIST (National Institute of Standards and Technology), U.S. Department of Commerce. https://webbook.nist.gov/chemistry/.
[27] Luning Prak DJ, Cowart JS, Trulove PC. Density, viscosity, speed of sound, bulk modulus, and surface tension of binary mixtures of n-Heptane + 2,2,4 Trimethylpentane at (293.15 to 338.15) K and 0.1 MPa. J Chem Eng Data 2014;59 (11):3842–51.
[28] Squillacote AH. The Paraview Guide. A parallel visualization application. Kitware, Inc; 2007.